

# TMI-CLNET: TRIPLE-MODAL INTERACTION NETWORK FOR CHRONIC LIVER DISEASE PROGNOSIS FROM IMAGING, CLINICAL, AND RADIOMIC DATA FUSION

Linglong Wu<sup>1,†</sup>, Xuhao Shan<sup>1,†</sup>, Ruiquan Ge<sup>1,\*</sup>, Ruoyu Liang<sup>2</sup>, Chi Zhang<sup>2</sup>,  
Yonghong Li<sup>3</sup>, Ahmed Elazab<sup>4</sup>, Huoling Luo<sup>3,7</sup>, Yunbi Liu<sup>5</sup>, Changmiao Wang<sup>6,\*</sup>

<sup>1</sup>Hangzhou Dianzi University, China    <sup>2</sup>The Chinese University of Hong Kong, Shenzhen, Shenzhen, China

<sup>3</sup>Shenzhen Institute of Information Technology, China    <sup>4</sup>Shenzhen University, China

<sup>5</sup>Nanjing University of Posts and Telecommunications, China    <sup>6</sup>Shenzhen Research Institute of Big Data, China

<sup>7</sup>Shenzhen Institute of Advanced Technology, Chinese Academy of Sciences, Shenzhen, China

## ABSTRACT

Chronic liver disease represents a significant health challenge worldwide and accurate prognostic evaluations are essential for personalized treatment plans. Recent evidence suggests that integrating multimodal data, such as computed tomography imaging, radiomic features, and clinical information, can provide more comprehensive prognostic information. However, modalities have an inherent heterogeneity, and incorporating additional modalities may exacerbate the challenges of heterogeneous data fusion. Moreover, existing multimodal fusion methods often struggle to adapt to richer medical modalities, making it difficult to capture inter-modal relationships. To overcome these limitations, We present the Triple-Modal Interaction Chronic Liver Network (TMI-CLNet). Specifically, we develop an Intra-Modality Aggregation module and a Triple-Modal Cross-Attention Fusion module, which are designed to eliminate intra-modality redundancy and extract cross-modal information, respectively. Furthermore, we design a Triple-Modal Feature Fusion loss function to align feature representations across modalities. Extensive experiments on the liver prognosis dataset demonstrate that our approach significantly outperforms existing state-of-the-art unimodal models and other multi-modal techniques. Our code is available at <https://github.com/Mysterwill/liver.git>.

**Index Terms**— Multi-modal Learning, Cross Attention, Radiomics, Chronic Liver Disease

## 1. INTRODUCTION

Chronic liver disease poses a significant threat to human health and safety. Chronic hepatitis caused by viral infections of hepatitis B virus (HBV) and hepatitis C virus (HCV) may progress to cirrhosis and hepatocellular carcinoma (HCC) [1]. Therefore, providing clinicians with timely and accurate prognostic results to guide early interventions

and treatment decisions is of critical importance in mitigating the health burden of chronic liver diseases. In clinical practice, patients present various non-imaging data including demographic information, complete blood count reports, and lipid analysis reports alongside routine imaging examinations such as Computed Tomography (CT). Meanwhile, radiomics can extract quantitative features from medical imaging data to describe disease characteristics. By integrating comprehensive domain knowledge with auxiliary information, we can develop a holistic and precise prognostic model for chronic liver disease, thereby offering robust support for clinical practice.

Numerous studies have explored multimodal approaches across various fields [2], often merging different modalities through simple concatenation or attention mechanisms [3, 4]. However, these conventional methods fail to accurately capture the intricate relationships between different modalities and struggle when dealing with a larger number of data types, thereby falling short of the demands of more complex datasets.

To address the challenges, we pioneeringly introduce a multimodal approach for prognosis assessment in chronic liver disease. Our work makes three notable contributions: (1) To our knowledge, this is the pioneering study to simultaneously integrate CT imaging, radiomic features, and clinical information into a unified multi-modal learning framework. (2) We design a unique TCAF module to address the heterogeneity among different modalities. This module effectively extracts cross-modal information to generate comprehensive global feature representations. (3) We introduce a TMFF loss to align feature representations across these three modalities during training, ensuring consistent semantic matching.

## 2. METHODOLOGY

The overall architecture of our network, as illustrated in Figure 1, consists of three main components: a feature extraction module, a multi-modal interaction module, and a classifica-

<sup>†</sup> These authors contributed equally to this work.

\*Correspondings: gespring@hdu.edu.cn, cmwangalbert@gmail.com.

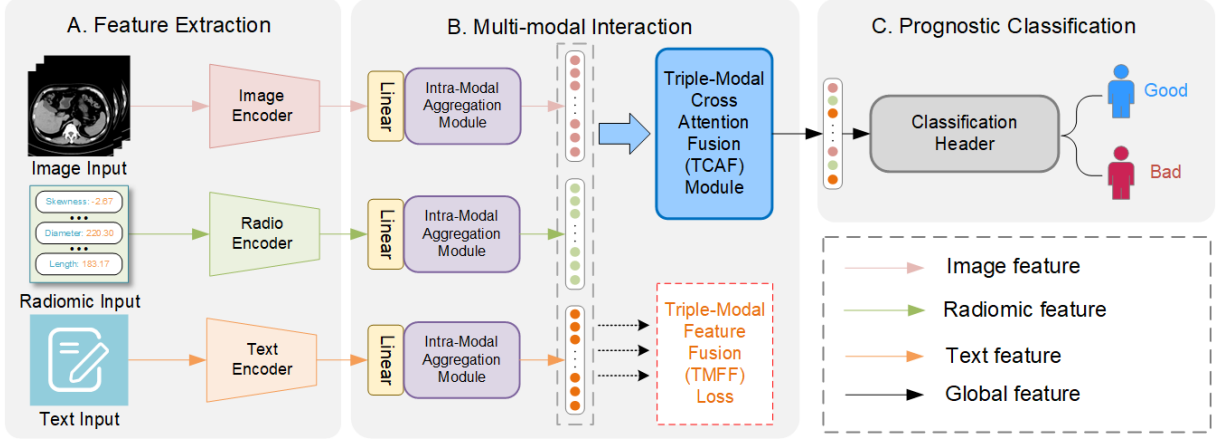


**Fig. 1:** Overview of our proposed TMI-CLNet. Given the CT scans, radiomic features, and clinical text, we feed them into an independent modal encoder to extract high-dimensional features. Subsequently, these features are fused through multi-modal interaction to incorporate global characteristics for prognosis classification. Simultaneously, the TMFF loss is employed to align multi-modal features.

tion head module.

In the feature extraction module, we employed a pre-trained 3D ResNet-50 as the visual encoder to extract deep visual features [5]. The radiomics data were tensorized and then processed using a Multilayer Perceptron (MLP) as the radiomics encoder to achieve more abstract feature representations. For clinical text, we utilized a pre-trained BioBERT model as the text encoder, selecting the output of the last hidden layer as the text feature representation [6]. In the classification head module, a pre-trained 1D DenseNet-121 is employed as the classification head.

## 2.1. Multi-modal Interaction Module

In this module, we employed linear layers from the outset to map the high-dimensional features obtained from the feature extraction module to a uniform size. Following this, the normalized high-dimensional features are processed by the Intra-Modal Aggregation (IMA) module to enhance their quality. At the core of the IMA is a multi-head self-attention mechanism with 16 attention heads. The primary role of the IMA is to consolidate intra-modal information before feature fusion, thereby improving the effectiveness of the fusion process and enhancing the overall performance of the model.

## 2.2. Triple-modal Cross-Attention Fusion Module

The architecture of this module is illustrated in Figure 2. After processing through the IMA module, the enhanced features from different modalities pass through linear layers to calculate their respective query  $Q$ , key  $K$ , and value  $V$  components for attention computation. The  $Q$  of each modality is multiplied by the transposed  $K$  of the adjacent modality, followed by a softmax layer. This result is then multiplied by the  $V$  of the adjacent modality to compute the attention

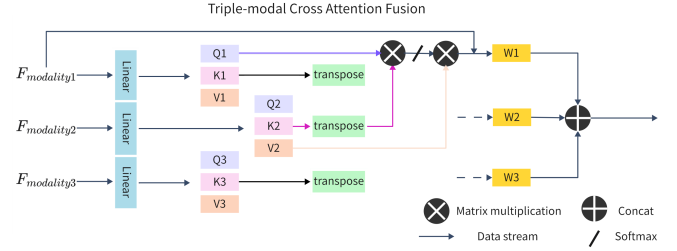


**Fig. 2:** Overview of our proposed TCAF module. The highlighting the process by the independent features from Modality 1 are integrated to produce cross-modal features.

scores for the given modality. Formally, this can be expressed as:

$$F_{hidden}^i = \text{softmax}\left(\frac{Q_i K_j}{\sqrt{d_k}}\right) V_j, j = i \bmod 3 + 1, \quad (1)$$

where  $i$  and  $j$  represent the index of the modality,  $d_k$  is the dimensions of the vector  $K$ . Moreover,  $a \bmod n$  represents the remainder of  $a$  divided by  $n$ . This is because the third modality interacts with the first modality through computational operations. Subsequently, to retain the original independent feature information, the attention scores ( $F_{hidden}^i$ ) are combined with the initial features ( $F_{modality}^i$ ) through concatenation. This combined output is then multiplied by a learnable weight matrix ( $W^o$ ).

This procedure is applied consistently to inputs from the three different modalities. Ultimately, the results are concatenated to produce the global feature output ( $F_{global}$ ). Mathematically, this can be represented as:

$$F_{global} = \bigoplus_{i=1}^n W_i^o (F_{hidden}^i \oplus F_{modality}^i). \quad (2)$$

This ensures that the connected features effectively serve as the comprehensive global feature representation.

### 2.3. Loss Function

**TMFF Loss.** To align features across different modalities, we drew inspiration from the Similarity Distribution Matching (SDM) loss [7] and developed a TMFF loss specifically for clinical texts, radiomics, and deep image features. The SDM loss was originally designed for the global alignment of visual and textual embeddings and is defined as:

$$\mathcal{L}_{v2t} = KL(\mathbf{p}_i \| \mathbf{q}_i) = \frac{1}{n} \sum_{i=1}^n \sum_{j=1}^n p_{i,j} \log \left( \frac{p_{i,j}}{q_{i,j}} \right), \quad (3)$$

where  $q$  denotes the genuine matching probability, and  $p$  represents the fraction of a particular cosine similarity score relative to the total sum. The bidirectional SDM loss aggregates both  $v2t$  and  $t2v$  losses. Thus, the SDM loss between visual and textual modalities can be described as:

$$\mathcal{L}_{SDM}^{vt} = \mathcal{L}_{v2t} + \mathcal{L}_{t2v}. \quad (4)$$

To align the features of the three modalities, we computed their pairwise SDM losses:  $\mathcal{L}_{SDM}^{it}$  (images and text),  $\mathcal{L}_{SDM}^{rt}$  (radiomics and text), and  $\mathcal{L}_{SDM}^{ir}$  (images and radiomics). Given the asymmetry of the SDM loss across different modality pairs and the similarity between image and radiomics features, aligning images with text should correspond to aligning radiomics with text. Therefore, we define the TMFF loss as follows:

$$\mathcal{L}_{multi} = \lambda \left( \frac{\mathcal{L}_{SDM}^{it} + \mathcal{L}_{SDM}^{rt}}{2} \right) + (1 - \lambda) \mathcal{L}_{SDM}^{ir}, \quad (5)$$

where  $\lambda \in [0, 1]$  is a scalar weight coefficient that controls the relative importance of the alignment terms.

**Overall Loss Function.** We employ a joint loss function to optimize the entire TMI-CLNet network. The overall loss function is formulated as a weighted sum of the task-specific and the multi-modal alignment losses. Mathematically, this can be expressed as:

$$\mathcal{L}_{total} = \mathcal{L}_{task} + \alpha \mathcal{L}_{multi}, \quad (6)$$

where  $\mathcal{L}_{task}$  is the commonly used cross-entropy loss function, and  $\alpha$  is a weighting hyperparameter that balances the contributions of  $\mathcal{L}_{task}$  and  $\mathcal{L}_{multi}$ . The value of  $\alpha$  is determined experimentally, with a typical value set to 1.

## 3. EXPERIMENTS

### 3.1. Experimental Setup

**Dataset.** Our study utilized a private liver prognosis dataset provided by a partner hospital, comprising 184 patients with

**Table 1:** Comparison with other methods using different modality configurations.

Method	Modality	ACC (%)	Precision (%)	Recall (%)	F1 Score	AUC
Resnet-50 [8]	Image	76.67	80.69	58.36	0.6718	0.7354
ViT [9]	Image	63.33	58.81	29.75	0.3270	0.5933
SVM [10]	Radiomic	57.01	47.72	39.34	0.4289	0.5718
RF [11]	Radiomic	66.22	61.82	49.98	0.5485	0.6828
SimpleFF [12]	I+R	72.75	74.72	54.10	0.6218	0.7050
HFBSurv [13]	I+R+C	79.45	82.01	64.32	0.7233	0.8015
MMD [14]	I+R+C	77.22	81.25	60.63	0.6772	0.7344
<b>TMI-CLNet (Our)</b>	<b>I+R+C</b>	<b>83.12</b>	<b>84.38</b>	<b>74.28</b>	<b>0.7805</b>	<b>0.8223</b>

109 indicating good and 75 bad prognoses. For each patient, we obtained corresponding CT images, quantitative radiomics data, and diverse clinical information. The CT images were first preprocessed in a common pipeline of window level selection and normalization, followed by resampling to dimensions of 64×512×512. The radiomics data extracted from the liver region encompassed 1,781 dimensions, covering aspects such as morphology, texture, and functionality. And all radiomic features were standardized to a unified range of -1 to 1. The clinical information included basic details such as gender, height, and Body Mass Index (BMI), a 23-dimensional Complete Blood Count (CBC) and biochemical index report, and a 16-dimensional fat analysis report.

**Implementation Details.** All experiments employed 5-fold cross-validation to validate the model’s stability and generalization capabilities. The batch size was set to 2, the learning rate to 0.0001, and the number of epochs to 300. The Adam optimizer was used for parameter optimization. All experiments were conducted using an NVIDIA A100 GPU.

### 3.2. Experimental Results

**Comparison with Other Methods.** Table 1 presents the comparative results of various methods. The first four methods rely on single-modal data as baselines, employing classic deep learning techniques such as ResNet50 [8] and ViT [9] for images, and machine learning techniques like Support Vector Machine (SVM) [10] and Random Forest (RF) [11] for radiomics data. The next three methods represent advanced approaches for handling multi-modal data. SimpleFF [12] sequentially integrates deep learning and radiomics data. HFBSurv [13] progressively fuses multi-modal data using a factorized bilinear model. Lastly, MMD [14] offers a universal framework for multi-modal feature fusion, accommodating both complete and missing modalities.

Integrating CT images with other modalities can sometimes degrade performance such as SimpleFF. This decline may be attributed to the inherent heterogeneity among different modalities, posing challenges for effective multi-modal feature fusion. In contrast, HFBSurv considers modality heterogeneity and cross-modal relationships, surpassing all single-modality methods. Our approach demonstrates superior performance across all metrics compared to other methods. Specifically, our framework achieved an accuracy of 83.12%, an F1 score of 0.7805 and an AUC of 0.8223. These results represent improvements of 3.67%, 0.0572, and

0.0208, respectively, over the best metrics from other methods.

**Ablation Study for Modalities.** Each experiment included the relevant encoders and classification heads. We used a direct connection for unimodal fusion, whereas, for bimodal fusion, we employed cross-attention mechanisms. As shown in Table 2, the results from the bimodal ablation experiments were similar to or slightly lower than those obtained with CT imaging alone. Specifically, the combination of vision and radiomics performed poorly, likely due to inconsistencies in the representation and dimensionality between deep features and handcrafted features, which simple cross-attention mechanisms are unable to effectively handle. However, our method achieved the best performance and this supports the effectiveness of our approach in handling modality heterogeneity and leveraging cross-modal information.

**Table 2:** Results of modal ablation experiment.

Method	ACC (%)	Precision (%)	Recall (%)	F1 Score	AUC
Vision-Only	77.68	78.53	64.98	0.6983	0.7541
Text-Only	73.33	74.91	54.21	0.6199	0.7001
Radio-Only	72.79	69.68	61.91	0.6459	0.7123
Vision+Text	76.64	71.43	68.75	0.6276	0.7224
Radio+Text	77.16	82.51	58.62	0.6707	0.7409
Vision+Radio	74.94	78.77	56.95	0.6341	0.7218
<b>TMI-CLNet (Our)</b>	<b>83.12</b>	<b>84.38</b>	<b>74.28</b>	<b>0.7805</b>	<b>0.8223</b>

**Ablation Study for IMA and TCAF.** To further validate the effectiveness of our modules in reducing intra-modality redundancy and extracting cross-modal information, we conducted ablation experiments on the IMA and TCAF modules. The results, presented in Table 3, show a significant performance improvement when each module was integrated individually. When both IMA and TCAF modules were used together, the accuracy increased by 7.64%. These results demonstrate that the network effectively integrates multi-modal information when all modules are applied, highlighting the strength of our approach in handling complex data.

**Table 3:** Ablation studies of important modules.

IMA	TCAF	ACC (%)	Precision (%)	Recall (%)	F1 Score	AUC
-	-	75.48	75.12	63.34	0.6504	0.6952
	✓	78.89	82.79	62.92	0.7019	0.7686
✓		81.47	83.94	68.55	0.7491	0.7883
✓	✓	<b>83.12</b>	<b>84.38</b>	<b>74.28</b>	<b>0.7805</b>	<b>0.8223</b>

**Ablation Study for Loss Weights.** In the TMFF loss, we introduce weight coefficients  $\lambda$  to control the relative importance of individual pairwise SDM losses. This ablation study examines the impact of different weight coefficients. The experimental results are shown in Table 4, where “-” indicates the absence of TMFF loss. By employing the TMFF loss and adjusting the coefficients  $\lambda$  to 0.2, 0.4, 0.6, and 0.8, we observe varying degrees of performance improvements. When  $\lambda$  is set to 0.6, our model surpasses the baseline without TMFF loss by 6.45% in accuracy and 0.0687 in AUC. These results underscore the significance of TMFF loss in aligning and

tegrating features across different modalities.

**Table 4:** Ablation studies of weight coefficients  $\lambda$  in the TMFF Loss.

$\lambda$	ACC (%)	Precision (%)	Recall (%)	F1 Score	AUC
-	76.61	73.42	68.36	0.7050	0.7536
0.2	80.95	79.66	<b>75.13</b>	0.7636	0.8017
0.4	78.21	76.93	67.33	0.7141	0.7668
0.6	<b>83.12</b>	84.38	74.28	<b>0.7805</b>	<b>0.8223</b>
0.8	79.85	<b>87.31</b>	59.78	0.7028	0.7659

**Interpretative Visualization.** In this study, we utilized XGradCAM [15] to analyze the decision-making process of our proposed TMI-CLNet. We selected four intermediate layers of the visual encoder as target layers, averaged their class activation maps, and converted them into heatmaps. Compared to a purely visual encoder, our fusion network focuses more on the liver region and reduces attention to task-irrelevant tissue areas. This indicates that, guided by clinical and radiomic information, the model excels in extracting relevant features from CT data.

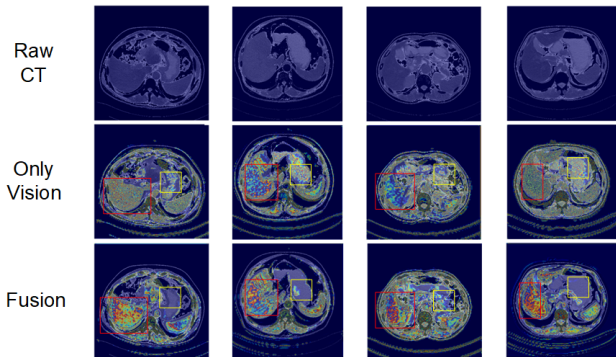


**Fig. 3:** Visual examples illustrating the model’s focus before and after fusion. The redder areas indicate higher model attention. Red boxes highlight the liver region, whereas yellow boxes denote areas deemed irrelevant by the model.

## 4. CONCLUSION

This study presented TMI-CLNet, which integrates CT imaging, radiomic features, and clinical information to provide early prognosis assessments for patients with chronic liver disease. By introducing the TCAF module and the TMFF loss function, the proposed model can address the heterogeneity among different modalities, thus achieving remarkable performance. Experimental results demonstrate the efficacy of our method. In the future, we will focus on expanding the dataset, conducting multi-center validation, and improving computational efficiency to enhance the robustness and scalability of the model. Additionally, our approach provides a valuable perspective and can be extended to other diseases or modalities, making it suitable for various future applications across different fields.

## 5. COMPLIANCE WITH ETHICAL STANDARDS

This study was conducted in accordance with the principles of the Declaration of Helsinki. Approval was granted by the Ethics Committee of Longgang Central Hospital of Shenzhen (2024.5.8/No.2024052).

## 6. ACKNOWLEDGMENTS

This work was supported by the Open Project Program of the State Key Laboratory of CAD&CG (No.A2410), Zhejiang University, Zhejiang Provincial Natural Science Foundation of China (No.LY21F020017), National Natural Science Foundation of China (No.61702146, 62076084), Guangdong Basic and Applied Basic Research Foundation (No.2022A1515110570), Innovation Teams of Youth Innovation in Science and Technology of High Education Institutions of Shandong Province (No.2021KJ088), and Guangdong Natural Science Foundation (No. 2023A1515012587).

## 7. REFERENCES

- [1] Marina Campos-Valdez, Manuel Alejandro Castro-García, Martha Eloísa Ramos-Márquez, Carmen Magdalena Gurrola-Díaz, Adriana María Salazar-Montes, and Laura Verónica Sánchez-Orozco, “An update on viral hepatitis b and c in mexico: Advances and pitfalls in eradication strategies,” *Microorganisms*, vol. 12, no. 7, pp. 1368, 2024.
- [2] Xinlei Yu, Ahmed Elazab, Ruiquan Ge, Jichao Zhu, Lingyan Zhang, Gangyong Jia, Qing Wu, Xiang Wan, Lihua Li, and Changmiao Wang, “Ich-prnet: A cross-modal intracerebral haemorrhage prognostic prediction method using joint-attention interaction mechanism,” *Neural Networks*, p. 107096, 2025.
- [3] Rayyan Azam Khan, Minghan Fu, Brent Burbridge, Yigang Luo, and Fang-Xiang Wu, “A multi-modal deep neural network for multi-class liver cancer diagnosis,” *Neural Networks*, vol. 165, pp. 553–561, 2023.
- [4] Xinlei Yu, Xinyang Li, Ruiquan Ge, Shibin Wu, Ahmed Elazab, Jichao Zhu, Lingyan Zhang, Gangyong Jia, Taosheng Xu, Xiang Wan, and Changmiao Wang, “Ich-pro: Intracerebral hemorrhage prognosis classification via joint-attention fusion-based 3d cross-modal network,” in *2024 IEEE International Symposium on Biomedical Imaging (ISBI)*, 2024, pp. 1–5.
- [5] Kensho Hara, Hirokatsu Kataoka, and Yutaka Satoh, “Can spatiotemporal 3d cnns retrace the history of 2d cnns and imagenet?,” in *Proceedings of the IEEE/CVF Conference on Computer Vision and Pattern Recognition*, 2018, pp. 6546–6555.
- [6] Jinhyuk Lee, Wonjin Yoon, Sungdong Kim, Donghyeon Kim, Sunkyu Kim, Chan Ho So, and Jaewoo Kang, “Biobert: a pre-trained biomedical language representation model for biomedical text mining,” *Bioinformatics*, vol. 36, pp. 1234 – 1240, 2019.
- [7] Ding Jiang and Mang Ye, “Cross-modal implicit relation reasoning and aligning for text-to-image person retrieval,” in *Proceedings of the IEEE/CVF Conference on Computer Vision and Pattern Recognition*, 2023, pp. 2787–2797.
- [8] Kaiming He, Xiangyu Zhang, Shaoqing Ren, and Jian Sun, “Deep residual learning for image recognition,” in *Proceedings of the IEEE/CVF Conference on Computer Vision and Pattern Recognition*, 2016, pp. 770–778.
- [9] Alexey Dosovitskiy, Lucas Beyer, Alexander Kolesnikov, Dirk Weissenborn, Xiaohua Zhai, Thomas Unterthiner, Mostafa Dehghani, Matthias Minderer, Georg Heigold, Sylvain Gelly, et al., “An image is worth 16x16 words: Transformers for image recognition at scale,” *arXiv preprint arXiv:2010.11929*, 2020.
- [10] Sovanlal Mukherjee, Anurima Patra, Hala Khasawneh, Panagiotis Korfiatis, Naveen Rajamohan, Garima Suman, Shounak Majumder, Ananya Panda, Matthew P. Johnson, N.B. Larson, Darryl E. Wright, Timothy L. Kline, Joel G. Fletcher, Suresh T. Chari, and Ajit H. Goenka, “Radiomics-based machine learning models can detect pancreatic cancer on prediagnostic cts at a substantial lead time prior to clinical diagnosis,” *Gastroenterology*, 2022.
- [11] L. Breiman, “Random forests,” *Machine Learning*, vol. 45, pp. 5–32, 2001.
- [12] Yoon Seong Choi, Sohi Bae, Jong Hee Chang, Seok-Gu Kang, Se Hoon Kim, Jinna Kim, Tyler Hyungtaek Rim, Seung Hong Choi, Rajan Jain, and Seung-Koo Lee, “Fully automated hybrid approach to predict the idh mutation status of gliomas via deep learning and radiomics,” *Neuro-oncology*, vol. 23, no. 2, pp. 304–313, 2021.
- [13] Ruiqing Li, Xingqi Wu, Ao Li, and Minghui Wang, “Hf-bsurv: hierarchical multimodal fusion with factorized bilinear models for cancer survival prediction,” *Bioinformatics*, vol. 38, no. 9, pp. 2587–2594, 2022.
- [14] Can Cui, Han Liu, Quan Liu, Ruining Deng, Zuhayr Asad, Yaohong Wang, Shilin Zhao, Haichun Yang, Bennett A Landman, and Yuankai Huo, “Survival prediction of brain cancer with incomplete radiology, pathology, genomic, and demographic data,” in *International Conference on Medical Image Computing and Computer-Assisted Intervention*. Springer, 2022, pp. 626–635.
- [15] Ramprasaath R Selvaraju, Michael Cogswell, Abhishek Das, Ramakrishna Vedantam, Devi Parikh, and Dhruv Batra, “Grad-cam: Visual explanations from deep networks via gradient-based localization,” in *Proceedings of the IEEE International Conference on Computer Vision*, 2017, pp. 618–626.